remote sensing

MDPI

Project Report

Monitoring Water and Energy Cycles at Climate Scale in the Third Pole Environment (CLIMATE-TPE)

Zhongbo Su [1,2], Yaoming Ma [3,*], Xuelong Chen [3], Xiaohua Dong [4], Junping Du [1], Cunbo Han [3], Yanbo He [5], Jan G. Hofste [1], Maoshan Li [6], Mengna Li [1], Shaoning Lv [7], Weiqiang Ma [3], María J. Polo [8], Jian Peng [9,10], Hui Qian [2], Jose Sobrino [11], Rogier van der Velde [1], Jun Wen [6], Binbin Wang [3], Xin Wang [12], Lianyu Yu [1], Pei Zhang [1], Hong Zhao [1], Han Zheng [2], Donghai Zheng [3], Lei Zhong [13] and Yijian Zeng [1]

1 Faculty of Geo-Information Science and Earth Observation (ITC), University of Twente, 7514 AE Enschede, The Netherlands; z.su@utwente.nl (Z.S.); 1@utwente.nl (J.D.); j.g.hofste@utwente.nl (J.G.H.); m.li-3@utwente.nl (M.L.); r.vandervelde@utwente.nl (R.v.d.V.); l.yu@utwente.nl (L.Y.); p.zhang@utwente.nl (P.Z.); h.zhao@utwente.nl (H.Z.); y.zeng@utwente.nl (Y.Z.)
2 Key Laboratory of Subsurface Hydrology and Ecological Effect in Arid Region of Ministry of Education, School of Water and Environment, Chang'an University, Xi'an 710054, China; qianhui@chd.edu.cn (H.Q.); zhenghan@chd.edu.cn (H.Z.)
3 Land-Atmosphere Interaction and Its Climatic Effects Group, State Key Laboratory of Tibetan Plateau Earth System, Resources and Environment (TPESRE), Institute of Tibetan Plateau Research, Chinese Academy of Sciences, Beijing 100101, China; x.chen@itpcas.ac.cn (X.C.); hcb@itpcas.ac.cn (C.H.); wqma@itpcas.ac.cn (W.M.); wangbinbin@itpcas.ac.cn (B.W.); zhengd@itpcas.ac.cn (D.Z.)
4 College of Hydraulic and Environmental Engineering, China Three Gorges University, Yichang 443002, China; xhdong@ctgu.edu.cn
5 National Meteorological Center, China Meteorological Administration, Beijing 100081, China; yanbohe@cma.gov.cn
6 Plateau Atmosphere and Environment Key Laboratory of Sichuan Province, College of Atmospheric Sciences, Chengdu University of Information Technology, Chengdu 610103, China; mshli@lzb.ac.cn (M.L.); jwen@cuit.edu.cn (J.W.)
7 Department of Atmospheric and Oceanic Sciences & Institute of Atmospheric Sciences, Fudan University, Shanghai 200433, China; lvshaoning@fudan.edu.cn
8 Grupo de Dinámica Fluvial e Hidrología, Universidad de Córdoba, 14071 Córdoba, Spain; ag1pogom@uco.es
9 Helmholtz Centre for Environmental Research—UFZ, Department of Remote Sensing, 04318 Leipzig, Germany; jian.peng@ufz.de
10 Remote Sensing Centre for Earth System Research, Leipzig University, 04318 Leipzig, Germany
11 Global Change Unit, Departament de Termodinamica, Facultat de Fisica, Universitat de Valencia, 46010 Valencia, Spain; Jose.Sobrino@uv.es
12 Key Laboratory of Land Surface Process and Climate Change in Cold and Arid Regions, Northwest Institute of Eco-Environment and Resources, Chinese Academy of Sciences, Lanzhou 730000, China; xinwang@lzb.ac.cn
13 School of Earth and Space Sciences, University of Science and Technology of China, Hefei 230026, China; zhonglei@ustc.edu.cn
* Correspondence: ymma@itpcas.ac.cn

Citation: Su, Z.; Ma, Y.; Chen, X.; Dong, X.; Du, J.; Han, C.; He, Y.; Hofste, J.G.; Li, M.; Li, M.; et al. Monitoring Water and Energy Cycles at Climate Scale in the Third Pole Environment (CLIMATE-TPE). *Remote Sens.* **2021**, *13*, 3661. https://doi.org/10.3390/rs13183661

Academic Editors: Jean-Pierre Wigneron, Kevin Tu and Christopher R. Hain

Received: 27 April 2021
Accepted: 2 September 2021
Published: 13 September 2021

Abstract: A better understanding of the water and energy cycles at climate scale in the Third Pole Environment is essential for assessing and understanding the causes of changes in the cryosphere and hydrosphere in relation to changes of plateau atmosphere in the Asian monsoon system and for predicting the possible changes in water resources in South and East Asia. This paper reports the following results: (1) A platform of in situ observation stations is briefly described for quantifying the interactions in hydrosphere-pedosphere-atmosphere-cryosphere-biosphere over the Tibetan Plateau. (2) A multiyear in situ L-Band microwave radiometry of land surface processes is used to develop a new microwave radiative transfer modeling system. This new system improves the modeling of brightness temperature in both horizontal and vertical polarization. (3) A multiyear (2001–2018) monthly terrestrial actual evapotranspiration and its spatial distribution on the Tibetan Plateau is generated using the surface energy balance system (SEBS) forced by a combination of meteorological and satellite data. (4) A comparison of four large scale soil moisture products to in situ measurements is presented. (5) The trajectory of water vapor transport in the canyon area of

Southeast Tibet in different seasons is analyzed, and (6) the vertical water vapor exchange between the upper troposphere and the lower stratosphere in different seasons is presented.

Keywords: Third Pole Environment; Tibetan Plateau; monsoon; earth observation; evaporation; soil moisture; microwave remote sensing

1. Introduction

The seasonal heating on the Tibetan Plateau has been thought to exert important controlling effects on the evolution of the Asian monsoon, which in turn controls the precipitation, weather and climate in South and East Asia (e.g., [1–5]) and affects the security of the water resources of 1.2 billion people in Asia. The snow depth on the Tibetan Plateau has been similarly attributed as an important factor influencing the onset of the Asian monsoon [6,7]. Despite these progresses in modelling and analysis, it remains a major challenge to understand the role of the Tibetan plateau in the Asian monsoon, being it topographic or thermal heating [8,9].

However, due to the remoteness and difficult access to the many landscapes on the Tibetan Plateau, consolidated datasets describing the states of the plateau land and atmosphere are lacking for coherently analyzing and evaluating numerical model outputs, remote sensing products and investigating the mechanisms of land–atmosphere interactions. The authors of [10] have reported major uncertainties in coarse resolution satellite and model products of soil moisture based on in situ observations on the Tibetan Plateau. Analyses of the most sophisticated models used by ECMWF (European Centre for Medium-Range Weather Forecasts, see Annex A for a list of abbreviations) and NCEP (National Centers for Environmental Prediction) have revealed that major improvements are needed in order to adequately simulate the states and dynamics of soil moisture and temperature profiles as well as land–atmosphere interactions [11–14].

From the foregoing, it has become evident that only by consolidating in situ observation of processes, Earth observation of state variables and numerical analyses of the mechanistic links between the major processes in land–atmosphere interactions shall the role of the Tibetan Plateau in Asian monsoons be fully understood. Therefore, the CLIMATE-TPE project was proposed for 'Monitoring Water and Energy Cycles at Climate Scale in the Third Pole Environment'. The main aim of the CLIMATE-TPE project was to improve the understanding of the interactions between the Asian monsoon, the plateau surface (including its permafrost and lakes) and the Tibetan plateau atmosphere in terms of water and energy budgets. Because such understanding is essential for assessing and understanding the causes of changes in the cryosphere and the hydrosphere in relation to changes in the plateau atmosphere in the Asian monsoon system, it is also necessary for predicting the possible changes in water resources in the Third Pole Environment (TPE). In the following section, we first introduce the project aim, the specific objectives and the data used. The research approaches are introduced in Section 3, followed by results in Section 4. Section 5 provides an overall discussion, concludes the contributions of CLIMATE-TPE, and suggests future research directions.

2. Objectives, Earth Observation and Other Data

The CLIMATE-TPE project used both satellite data and in situ measurements to advance process understanding covering the relevant monsoon scale and develop coupled regional scale hydroclimatic models to explain different physical links that cannot be observed directly. Specific objectives focused on the advancement of knowledge in three challenges and were organised into three sub-projects.

Objective (1) Advancement of the understanding of microwave scattering and emission under complex terrains with permafrost and freeze–thawing cycles.

The focus was to reduce uncertainties in microwave satellite observations over complex terrain and improve retrieval accuracies of soil moisture and freeze-thaw states by deploying in situ observations, laboratory experiments and numerical modelling.

Objective (2) Advancement of physical understanding and quantification of water and energy budgets in the TPE.

The focus here was to integrate current understandings in the mechanism of changes in water and energy budget in TPE using satellite data products and numerical modelling.

Objective (3) Advancement of quantifying changes in surface characteristics and monsoon interactions.

Relevant variables related to water and energy budgets in TPE were subject to systematic analysis to ensure their consistency in terms of climate data records. The variables included albedo, vegetation coverage, soil thermal and hydraulic properties, land surface temperature (LST), soil moisture, lake levels and land use changes, among others.

The CLIMATE-TPE project used ESA Earth Observation (EO) data (ERS, ENVISAT and Earth Explorer mission data), Chinese EO data and ESA Third Party Mission (TPM) data, including additional data collected from in situ sensors, operational meteorological data and numerical model outputs. Table 1 provides a description and summary of used EO data and other data.

Table 1. Summary of EO data and other data used in CLIMATE-TPE.

ESA EO Data	Chinese EO Data	ESA TPM and Other Data
○ ENVISAT MERIS, AATSR, ASAR level 1b data for detailed analysis at selected experimental sites for algorithm development and validation. ○ ENVISAT MERIS, AATSR, ASAR level 2 data (ASAR Global Monitoring modes) for Analysis of all data products related to water and energy cycle components. ○ SMOS data ○ Sentinel 1/2 data as well as Sentinel-3 data	FY SERIES ○ Multi-channel Visible and Infrared Spin Scan Radiometer (VISSR) (FY-2C/2D). ○ FY-3 data subject to availability	○ ALOS data for validation sites ○ TERRA/AQUA-MODIS ○ SMAP data ○ Nationwide meteorological data (historical and real time data) (CNMC) ○ Experimental database for all experimental sites (site PIs) ○ Reanalysis data (ERA-interim) from ECMWF and NCEP reanalysis data ○ DEM and soil maps over China ○ Vegetation cover maps over China and the TPE ○ In situ observation data from micrometeorological stations operated by ITP and CAREERI

3. Methods

Next, we describe the general methods we have used to ensure the consistency of the water and energy budgets at different spatial and temporal scales. The linkages between different water and energy cycle components can be described by the energy and mass conservation framework. The change in energy stored at land surface (S_e) is described as:

$$\frac{dS_e}{dt} = R_n - H - LE - G \quad (1)$$

where H is sensible heat flux, LE is latent heat flux (E is evaporation/transpiration and L is the latent heat of vaporization), G is ground heat flux and R_n is net radiation, which is calculated as:

$$R_n = (1 - \alpha)R_s^{\downarrow} + R_L^{\downarrow} - R_L^{\uparrow} \quad (2)$$

where $R_s^{\downarrow}$ is solar radiation, α is albedo, $R_L^{\downarrow}$ is atmospheric long-wave radiation flux incident on land surface and $R_L^{\uparrow}$ is long-wave radiation flux emanating from land surface. Similarly,

the change in the amount of water stored in a control volume equals to the net flow of water into and out of it is calculated as:

$$\frac{\partial S}{\partial t} = P - E - R_o - R_u \quad (3)$$

where S is the amount of moisture stored at and below the surface per unit of land surface, P is precipitation, E is evaporation, R_o is net surface runoff and R_u is net percolation of water as groundwater.

The energy and water balances at land surface are linked via the evaporation term, and Equations (1)–(3) form the basis for all land surface models. When mass conservation is applied to atmospheric and land water budgets together, the complete global water cycle can be considered. The atmospheric water balance can be described as:

$$\frac{\partial W}{\partial t} = Q + (P - E) \quad (4)$$

where W represents precipitable water and Q is convergence of water vapor flux in the atmosphere. Combining terrestrial and atmospheric water budgets in Equations (3)–(4), we obtain:

$$\frac{\partial W}{\partial t} - Q = P - E = \frac{\partial S}{\partial t} + R_o + R_u \quad (5)$$

Equation (5) states that the difference between precipitation and evaporation equals to the sum of decrease of atmospheric water vapor storage and horizontal convergence, and also to the sum of increase of water storage over land and runoff. This framework is the basis for examining the consistency of water and energy cycle variables derived from different data source.

In the CLIMATE-TPE project, we proposed three sub-projects organized as work packages (WP), and each WP is divided into a number of tasks to address linkages between different water cycle components in the energy and mass conservation framework given by Equations (1)–(5).

3.1. WP1: Observation and Modelling of Microwave Scattering and Emission under Complex Terrains including Permafrost and Freezing and Thawing

We deployed a L-band (1.41 GHz) radiometer (ELBARA-III, [15]) at the central micrometeorological station (latitude: 33.919750, longitude: 102.153183, WGS'84) of the Maqu network of the Tibetan Plateau since 2016. ELBARA-III was supported by ESA for experimental observation for the calibration and validation of SMOS (Soil Moisture and Ocean Salinity) data and products. The following tasks were defined and executed:

(1) We conducted ELBARA-III measurements since 2016, covering complete annual freezing–thawing cycles, for advancing understanding of the mass and energy exchanges involved in the freeze–thaw process [16].
(2) The collected ELBARA-III observations have been analysed with the recently developed effective temperature model [17] to better understand the microwave emission signals, including the validation of ESA's SMOS and NASA's SMAP radiometer brightness temperatures (T_B).
(3) The collected ELBARA-III and other in situ data have been used to develop microwave radiative transfer models to simulate existing satellite data of different frequencies (e.g., for low spatial resolution data SCAT/ASCAT, SSM/I, AMSR-E/2, SMOS and high spatial resolution data ASAR/S-1) [17–19]. This ensures the generation of a climatically consistent soil moisture data product by using the same consistent framework and contributes to the ESA Climate Change Initiative.
(4) A scatterometer system was installed next to the ELBARA-III system and performed measurements in the period August 2017–August 2018 over the 1–10 GHz frequency range. The scatterometer measurements provided complementary and additional

information on the surface freeze/thaw state and the influence of vegetation cover on its microwave signatures.

3.2. WP2: Advancement of Physical Understanding and Quantification of Water and Energy Budgets in TPE

The focus in this WP is to integrate current understandings in the mechanism of changes in water and energy budget in TPE using satellite data products and numerical modelling. The following tasks were defined and conducted:

(1) Observation and analysis of water and energy balance of the Namco Lake catchment area using the concept of water and energy balance closure (Equations (1)–(5)). An energy balance and micrometeorological station was established on the Namco Lake, and the observations were continued throughout the duration of the Dragon 4 programme [20]. The permanent Namco environmental observation station operated by ITP/CAS (Institute of Tibetan Plateau Research, Chinese Academy of Sciences) since 2005 on the adjacent land was used to construct the water cycle budgets of the lake catchment together with the lake observation, satellite observations and modelling.
(2) Advances in understanding land–atmosphere interactions with the Noah model at local scale [12–14] enabled the generation of consistent data sets for water and energy cycles in the TPE.
(3) Development of high-resolution land surface energy and water fluxes from satellite data using EO data (see Table 2).
(4) Joint diagnoses of the products from tasks (2)–(3) were conducted to improve model physics, parameterisation and parameters for climate analysis.
(5) The STEMMUS-FT model was developed to understand the detailed freeze–thaw dynamics across the soil profile, considering the coupled process of liquid, vapor, air and heat transfer, as well as soil ice formation [21,22]. The STEMMUS-FT model is further coupled with the COSMIC model to assimilate Cosmic Ray Neutron Counts for determining soil ice content at field scale (~200 m^2) [23]. This field scale provided a representative footprint to compare with the ELBARA-III observations.

3.3. WP3: Advancement in Quantifying Changes in Surface Characteristics and Monsoon Interactions

Variables related to water and energy budgets in TPE were subject to systematic analysis to ensure their consistency in terms of climate data records. The variables included albedo, vegetation coverage, soil thermal and hydraulic properties, LST, soil moisture, lake levels and vegetation changes among others.

(1) Analysis of existing climate data records and essential climate variables (CDR/ECV) data (e.g., those from ESA CCI) with the validation framework proposed in the EU CORE-CLIMAX project by [24,25];
(2) Generating new and consistent land surface variables for the TPE, including, in particular, LST, soil moisture and soil thermal and hydraulic properties (see Table 2, [26]);
(3) Integration of these new consistent datasets into the research of WP2;
(4) Assimilation of microwave observation from SMOS and SMAP into the WRF modelling system using the concept of observing depth of microwave sensing [17,27];
(5) Analysis of monsoon dynamics in relation to changes of plateau surface characteristics by using the WRF modelling system.

Table 2. List of main results obtained in CLIMATE-TPE.

WP	Results
WP 1: Observation and modelling of microwave scattering and emission under complex terrains including permafrost and freeze and thawing	A data record of L-band radiometry [16] A data record of 1–10 GHz scatterometry [28] Analysis results of ELBARA observations [29,30] New retrieval methods by merging existing satellite data of different frequencies PhD theses
WP2: Advancement of physical understanding and quantification of changes of water and energy budgets in TPE	Results of observation and analysis of water and energy balance of the lakes in TPE [31] A consistent soil moisture data set for the Tibetan Plateau [32–34] A high-resolution land surface energy and water fluxes from satellite data using EO data using the SEBS model [35,36] Results of joint diagnoses of the products from (2)–(3) were conducted to improve model physics, parameterisation and parameters for climate analysis A STEMMUS-FT model for detailing freeze-thaw dynamics [21,22] PhD theses
WP3: Advancement of quantifying changes in surface characteristics and monsoon interactions	Results of analysis and validation of existing CDR/ECV data (e.g., those from ESA CCI) [37] A set of new and consistent land surface variables for the TPE (LST, soil moisture, soil thermal and hydraulic properties) Integration of these new consistent dataset into research of WP2 (see results under WP2) Development of observation operators for assimilation of microwave observation from SMOS and SMAP into the modelling system Analysis of monsoon dynamics in relation to changes of plateau surface characteristics [38] PhD theses

4. Selected Project Results

The CLIMATE-TPE project has obtained numerous results that are summarized in Table 2.

In the following, we present some examples that highlight some of the achieved results.

4.1. In Situ Observation Stations (Sites) of Hydrosphere–Pedosphere–Atmosphere–Cryosphere–Biosphere Interactions over the Tibetan Plateau

A unique integrated network platform to study the multi-sphere (hydrosphere–pedosphere–atmosphere–cryosphere–biosphere) interactions was set up since 2011 over the entire Tibetan Plateau ([39]; Figure 1). The platform includes 10 multi-sphere stations, 21 air-land flux exchange stations, 10 multi-sphere sites, 3 soil moisture and soil temperature networks, 5 radiosonde stations, 6 glacier monitoring sites, 3 lake monitoring sites and 8 isotope monitoring sites. All instruments collected continuous observations for about 10 years, including an intensive observation period from May to October 2011. Additionally, a comprehensive three-dimensional observation experiment (satellite-airborne flight-field observation) was carried out in the Qiangtang Plateau and the water vapor channel in the southeast plateau. In the framework of Dragon 4, large amounts of multi-sphere data were collected to create a database to study the interactions between the Asian monsoon, the plateau surface and the plateau atmosphere in terms of water and energy budgets [40].

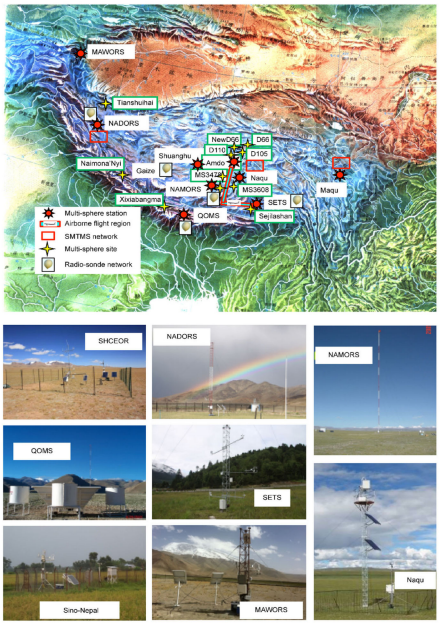

Figure 1. Spatial distribution of observation stations (sites) of hydrosphere–pedosphere–atmosphere–cryosphere–biosphere interactions over the Tibetan Plateau (**top panel**) and the typical observation instruments for different land surfaces (**bottom panel**) (Source: [40]).

4.2. Multiyear In Situ L-Band Microwave Radiometry of Land Surface Processes

We collected a multiyear in situ radiometry dataset which includes measurements of the L-band brightness temperature, the profile of the soil moisture and soil temperature, CO_2/H_2O fluxes and meteorological data, as well as auxiliary vegetation and soil texture information [16]. The dataset has been used to advance the understanding of the scattering-emission mechanism of vegetated lands [29] and to study the L-band microwave emission of frozen soil during the thawing period [41].

Topsoil structures and the inhomogeneous distribution of moisture in the soil volume induce dielectric discontinuities from air to bulk soil, which in turn may induce volume scattering and affect the microwave surface emission. The above data were exploited to understand the effect of surface roughness on coherent and incoherent emission processes and resulted in an air-to-soil (ATS) model [29]. The ATS model incorporates the dielectric roughness characterized by soil moisture and geometric roughness effects (i.e., those resulted from small-scale topsoil structures and the soil moisture profile in the soil volume). The ATS model was then coupled to the advanced integral equation model (AIEM) [42,43] for soil surface scattering with a discrete scattering-emission model for vegetation (TVG, known as the Tor Vergata model) [44] (henceforth, ATS-AIEM-TVG) for modelling the overall vegetation-soil scattering-emission processes. The integrated ATS-AIEM-TVG model can adequately simulate the seasonal and diurnal variations of the brightness temperature and help to physically interpret the involved processes and mechanisms (Figure 2). However, the integrated model is not yet able to capture the dynamic change of land surface and soil conditions that undergo rapid freeze–thaw processes, and this is where the model simulation of brightness temperature starts to deviate from ELBARA-III observations (see Figure 2).

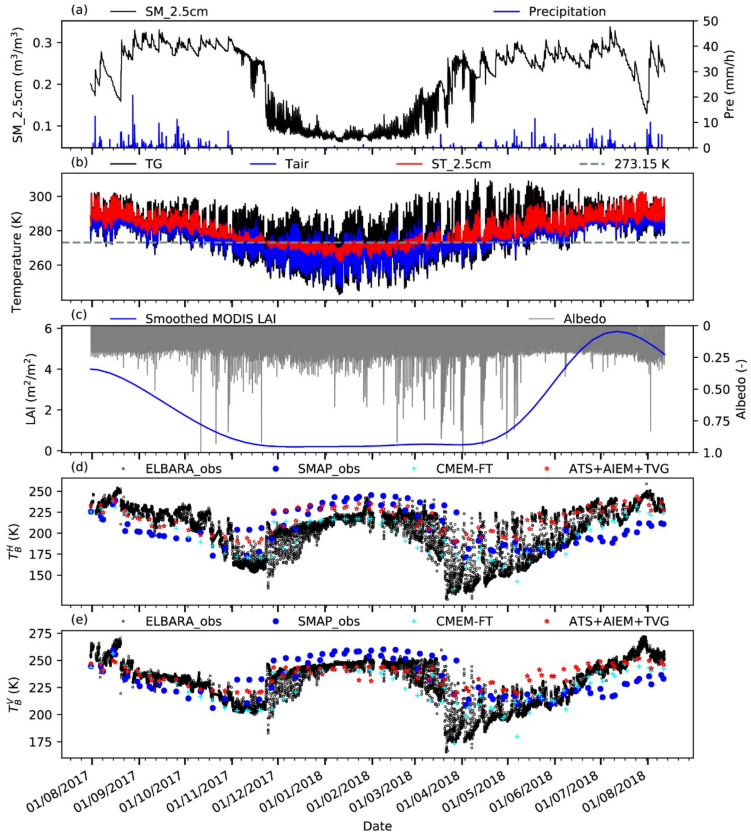

Figure 2. Seasonal variations of the Maqu ELBARA-III radiometry dataset between 1 August 2017–1 August 2018. Plotted are (**a**) soil moisture at 2.5 cm depth (SM_2.5 cm), precipitation, (**b**) ground surface temperature (TG), air temperature (Tair), soil temperature at 2.5 cm depth (ST_2.5 cm), the nominal freezing point as a reference (273.15 K), (**c**) leaf area index (LAI), albedo and (**d**) the brightness temperature intercomparison between ELBARA-III observations (ELBARA_obs), SMAP observations (SMAP_obs), CMEM-FT and ATS + AIEM + TVG simulations in horizontal polarization (T_B^H) at 40° incidence angle, and (**e**) the same as (**d**) but in vertical polarization (T_B^V).

Currently, the SMAP and SMOS missions provide global coverage of freeze–thaw (FT) states that characterize surfaces as either freeze or thaw with binary flags. However, the transition between freeze and thaw is a continuous process in space and time, especially for the L-band, whose penetration depth reaches tens of centimeters below the ground surface [30]. In this case, the SMAP and SMOS brightness temperature is a mixed signal of FT states over the footprint and is generated from a soil column that might encompass the freezing/thawing front. To model such complex states, we extended the community microwave emission modelling platform (CMEM) in Fresnel mode with the freezing/thawing component by allowing for: (1) a varying fraction of open water surface which may be modelled or estimated from surface temperature, and (2) implementing a freezing/thawing phase transition delay based on the difference in soil temperature at the surface and at a 2.5-cm depth. The augmented CMEM-FT is capable of capturing the brightness temperature dynamics from a completely frozen to a thawed state ([41], Figure 2).

4.3. Evaluation and Generation of Land Heat Fluxes and Evapotranspiration

Evapotranspiration (E) regulates the energy and hydrology cycle of land surface and links the land and atmospheric water and energy budgets. However, its magnitude remains highly uncertain at the global scale, and how to derive the reliable global E has been intensively debated in recent years. Among the multiple climate models which were included in Phase 6 of the Coupled Model Intercomparison Project (CMIP6), the estimations of the

global land *E* have a high discrepancy. The authors of [45] evaluated the global terrestrial *E* of CMIP6 models and reported that most CMIP6 models overestimated *E*, which might be caused by the overestimation of precipitation in CMIP6. Most CMIP6 models showed an increasing trend in *E* during the period from 1980–2014 due to significant increases in transpiration, which accounts for more than 60% of *E*, and the main influencing factor was the increase in LAI because of greening [46]. The CMIP6 ensemble mean underestimated *E* in regions with high evapotranspiration, such as the Amazon basin, central Africa and Southeast Asia, and overestimated *E* in regions with low evapotranspiration, such as the Sahara desert, the Middle East, southwest Australia, and the Andes Mountains. The generation of land heat fluxes and evapotranspiration independently based on satellite observations can help to reduce the uncertainties in these climate models.

In Figure 3, the multiannual (2005–2016) mean evaporation is displayed for different products for comparison, including SEBS [35,47,48], MOD16 [49], GLEAM [50], GLDAS [51] and ERA-Interim [52]. From the latitudinal averages, other model estimates are normally lower than that from GLDAS; SEBS is the most comparable to GLEAM despite their difference in forcings and model assumptions; while, GLEAM needs precipitation and soil moisture inputs, which makes it susceptible to the uncertainties of these inputs, SEBS mainly relies on direct satellite observation of land surface variables (albedo, LST and fractional vegetation coverage). Note that the main differences between these products relate to the choice of meteorological and radiation forcing.

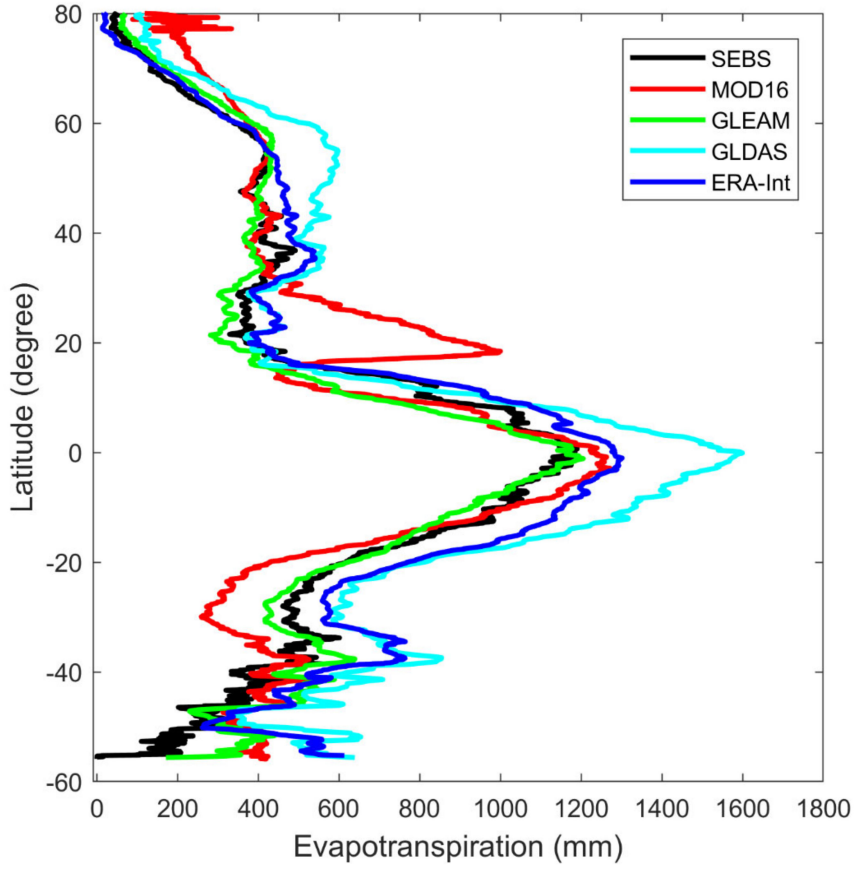

Figure 3. Comparison of latitudinal profiles of global evaporation by five data sets.

Next, we estimated the multiyear (2001–2018) monthly terrestrial actual evapotranspiration (*E*) and its spatial distribution on the Tibetan Plateau (TP) using the surface energy balance system (SEBS) forced by a combination of meteorological data and satellite products [53].

From the trend of annual E during 2001–2018 shown in Figure 4, a dominant increasing trend is detected in the eastern TP (lon > 90° E) while a decreasing trend is dominant in the western TP (lon < 90° E). The trends pass the t-test ($p < 0.05$) in most parts of the area. The decreasing trend in the western TP is pronounced and is larger than -7.5 mm yr^{-1} in most parts of the area and even larger than -10 mm yr^{-1} in a few parts. In the eastern TP, the increasing trend is mostly between 5 and 10 mm yr^{-1}. The E trend tends to be greater along the marginal region of the northern, eastern and southeastern TP. Along the marginal region of the southwestern TP and in the western section of Himalaya Mountains, this trend weakens.

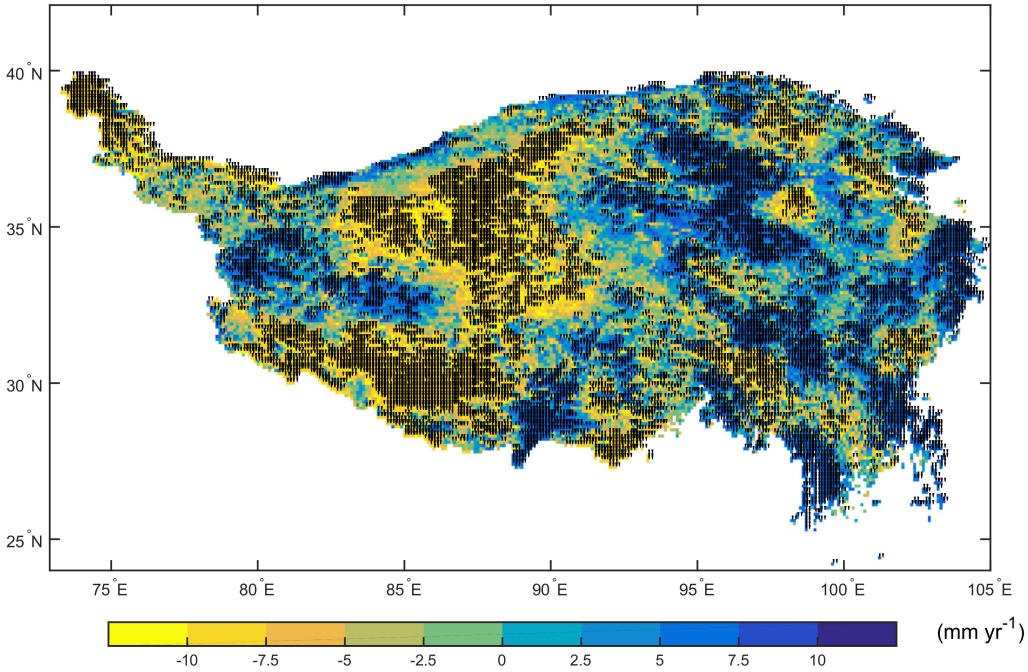

Figure 4. Spatial distribution of annual E linear trend on the TP from 2001 to 2018. The stippling indicates trends that pass the t-test ($p < 0.05$).

4.4. Climate Scale Monitoring of Soil Moisture and Soil Temperature and Validation of Large Scale Soil Moisture Products

The Tibetan plateau observatory of plateau scale soil moisture and soil temperature (Tibet-Obs) [10] has been continuously maintained and upgraded for climate scale monitoring of soil moisture and soil temperature and for quantifying uncertainties in coarse spatial resolution satellite and model products. Figure 5 shows examples of the comparisons between Tibet-Obs observations and some global products, including the reanalysis data ERA-interim [52] and ERA5 [54,55], the ESA Climate Change Initiative combined passive and active soil moisture data (CCI-combined) [56] and SMAP operational products [57–59]. The satellite data in general reflect the in situ observations in the monsoon period (June–September) in the desert areas (Ngari and Ali) but show systematic difference in semi-arid areas (Naqu). Except for the impact of vegetation in the cold humid area (Maqu), the new SMAP satellite data show in general better agreements than the CCI-combined products with the in situ observations. While the new reanalysis data (ERA5) is certainly better than ERA-Interim in the desert areas (Ngari and Ali), such improvements are not obvious for semi-arid (Naqu) and cold humid area (Maqu). These all point to the need to further improve these data products for climate monitoring and analysis [11,33].

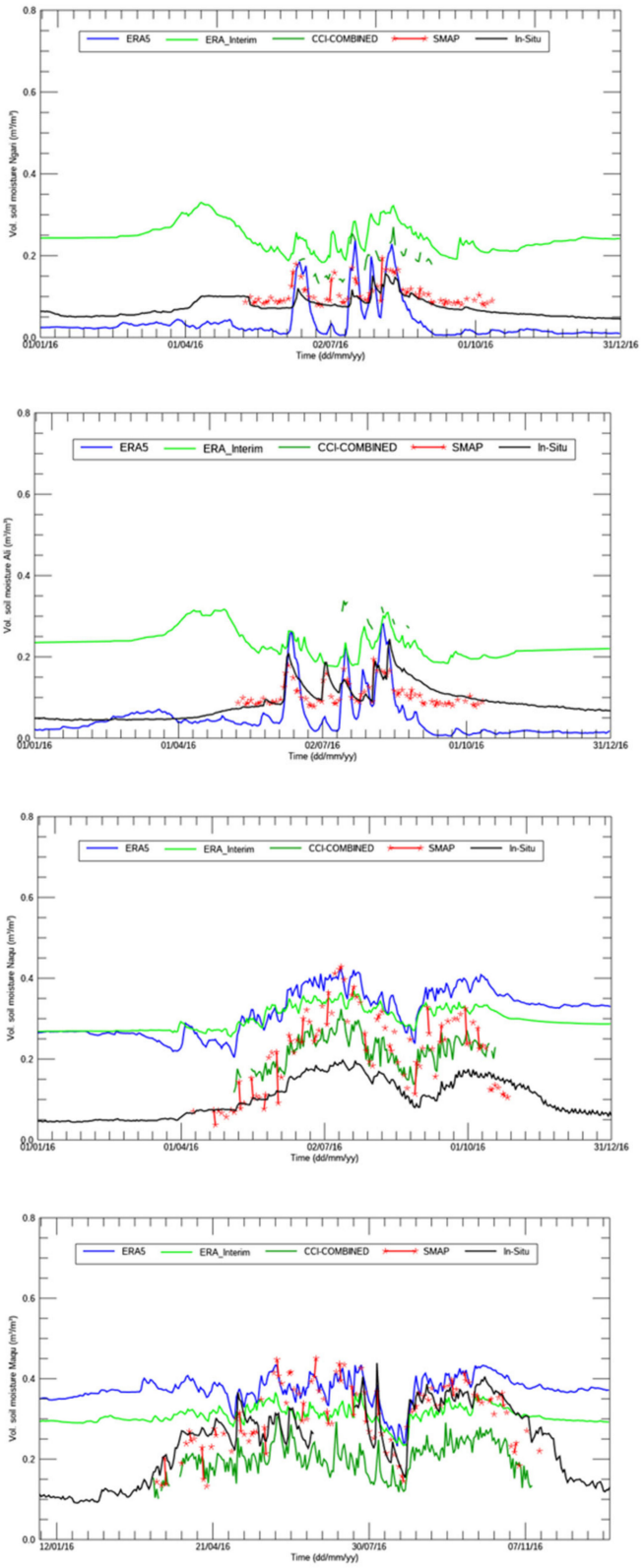

Figure 5. Comparisons between Tibet-Obs observations and four global soil moisture products at Ngari, Ali, Naqu and Maqu networks.

4.5. Trajectory of Water Vapor Transport in the Canyon Area of Southeast Tibet

To identify the trajectory of water vapor transport on the TP, reanalysis data from NCEP/NCAR were used with a resolution of 1° × 1° from October 2018 to November 2019.

The Hysplit4 backward trajectory model was used to simulate the 48-h backward air mass trajectory. Through cluster analysis, the source of water vapor transportation trajectory in different seasons in the southeast gorge of Tibet was obtained for the study area shown in Figure 6.

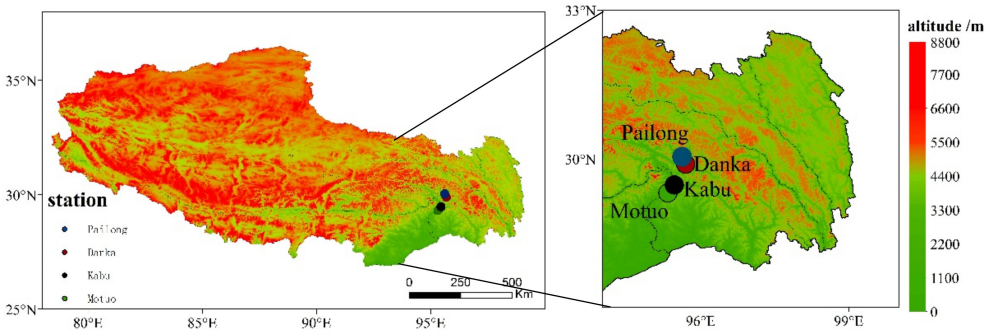

Figure 6. Southeast area of the Tibetan Plateau and the used observation stations (circles).

Figure 7 shows the 48-h water vapor transport trajectory at each of Pailong Station, Danka Station, Kabu Station and Motuo Station in spring. From these trajectories, it can be seen that the main source of water vapor transport in spring is zonal water vapor transport, and the water vapor channels are mainly westward and northwest airflows. At Pailong Station (Figure 7a), 11% of the water vapor comes from the northwest, 64% of the water vapor comes from the west, for which the 48-h backward trajectory can be traced back to Pakistan and Afghanistan, and 25% of the water vapor comes from the south. About 10% of the water vapor at Danka Station (Figure 7b) comes from the northwest, and 91% of the water vapor comes from the west airflow. More than 50% of the water vapor at the Kabu (Figure 7c) and Motuo (Figure 7d) stations comes from the southwest. The strong westerly wind in the southern part of the plateau in spring is the main water vapor transport channel in the Canyon Area of Southeast Tibet. The high terrain of the plateau has the effect of circumventing the westerly belt, forming a "southern trough and northern ridge". The northwest airflow from the northern ridge transports about 10% of water vapor to southeastern Tibet in spring. The height of the water vapor transmission channel to the southwest is below 2000 m, and while the height of the water vapor transmission channel to the west is basically above 3000 m, the water vapor transmission height of Danka and Motuo stations can reach 4500 m. The topography is closely related to the height of water vapor transport.

Compared with the sources of water vapor transport at various stations in spring, the main sources of water vapor transport in summer (Figure 8) change from the westward airflow to the southerly one, and the main water vapor comes from the Bay of Bengal and the South China Sea. Judging from the altitude and geographic location of each station, Pailong Station (Figure 8a) and Danka Station (Figure 8b) are located relatively north, Pailong Station is lower than Danka Station and there is still a northwesterly airflow. The Kabu (Figure 8c) and Motuo (Figure 8d) stations located to the south are low in altitude, and the height of the water vapor transmission channel in the northwest is lower than that in the spring, which prevents this part of water vapor from being transported to the south. Pailong Station and Danka station have 6% of the southeast air transport in summer, while Kabu and Motuo do not have this part of the source of water vapor. The southerly airflow at Kabu and Motuo stations exceeds 90% in summer, because the South Asian monsoon prevails on the plateau in summer. At this time, the southwest wind makes a major contribution to the transport of water vapor from the Bay of Bengal. A major water vapor transmission channel is formed over the southeastern Tibet to the inland areas. The height change characteristics of the westward and southward water vapor transmission channels in summer are the same as those in spring. The southeast water

vapor transmission channels of Pailong Station and Danka Station have a height of 3000 m to 3500 m.

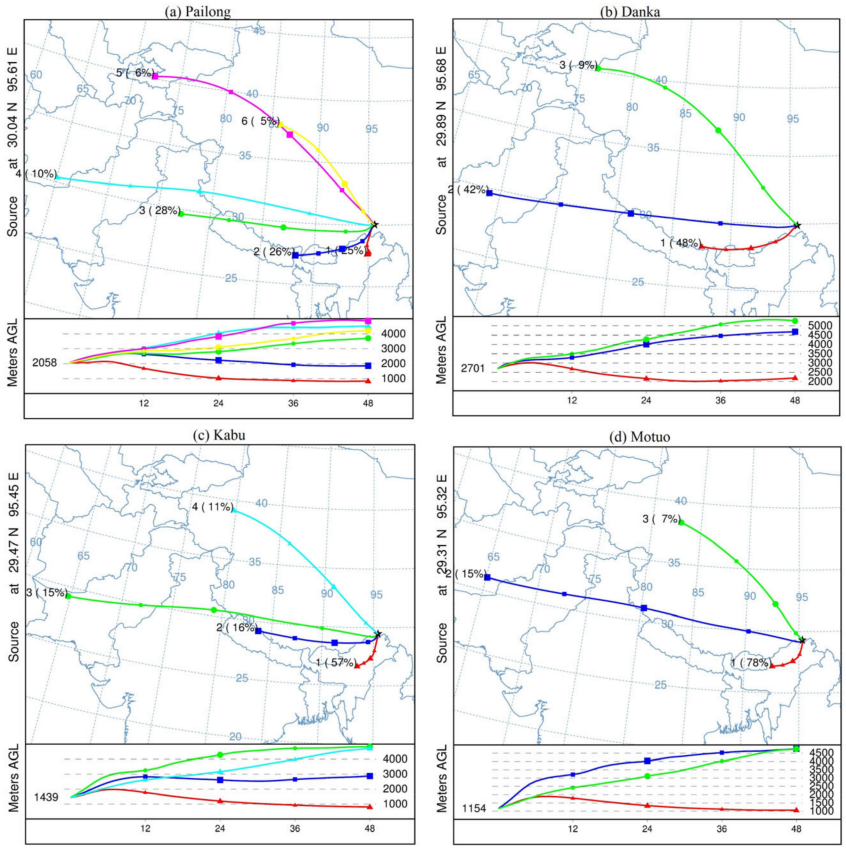

Figure 7. The 48-h water vapor transport trajectory at each station in spring. (**a**) Pailong station, (**b**) Danka station, (**c**) Kabu station, (**d**) Motuo station. (Meters AGL refers to the height in meters above ground level of the different trajectories).

Figure 9 shows the 48-h water vapor transport trajectory characteristics of each station in autumn. Compared with the situation in summer, the water vapor transmission channel to the southeast of Pailong Station (Figure 9a) and Danka Station (Figure 9b) disappeared, and the proportion of southerly airflow at each station decreased. However, the main channel for water vapor transport in the canyons of southeastern Tibet is still the southerly airflow, with each station reaching more than 60% and Kabu (Figure 7c) reaching 79%. The westerly wind on the plateau gradually began to strengthen in autumn, and the proportion of water vapor transported by the westerly airflow also gradually increased. The change characteristics of the height of each water vapor transmission channel are still obvious.

In winter, the westerly wind over the plateau gradually intensifies and reaches its maximum (Figure 10). The water vapor transport from the westward airflow increases. The source of water vapor in the 48-h backward direction from each station is farther than that in spring because of the strong westerly wind in winter. The height of the westward water vapor transmission channel is also higher than that in spring. There is a southeast water vapor transmission channel at Pailong Station (Figure 10a), Kabu Station (Figure 10c) and Motuo Station (Figure 10d). In winter, the mainland is dominated by a cold anticyclone, so there is a water vapor transmission channel in the southeast direction. The height of the channel is below 1000 m. However, this water vapor transmission channel does not occur at Danka Station due to the high altitude (Figure 10b).

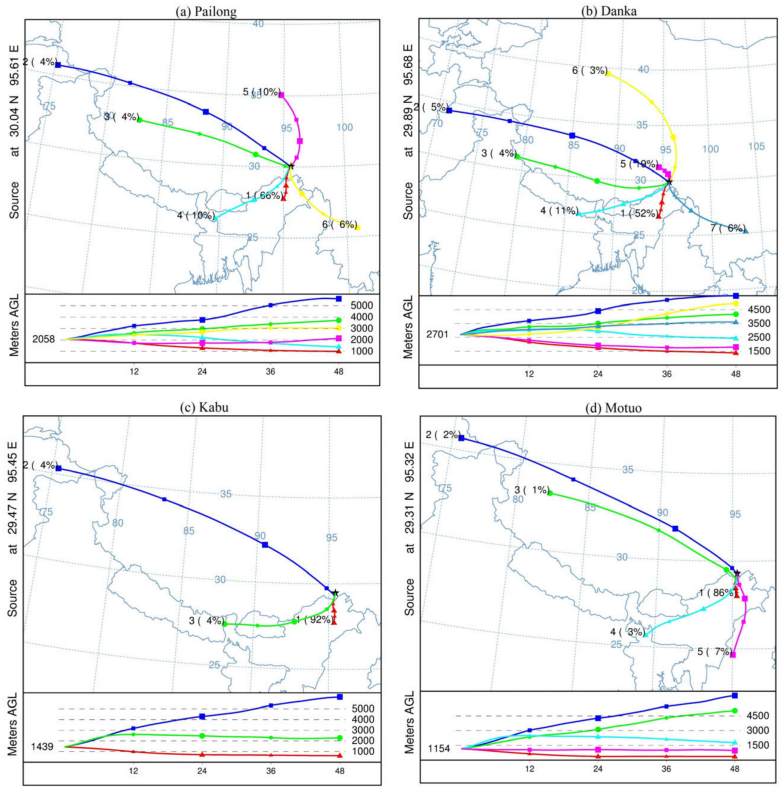

Figure 8. The same as Figure 7 but for each station in summer. (**a**) Pailong station, (**b**) Danka station, (**c**) Kabu station, (**d**) Motuo station.

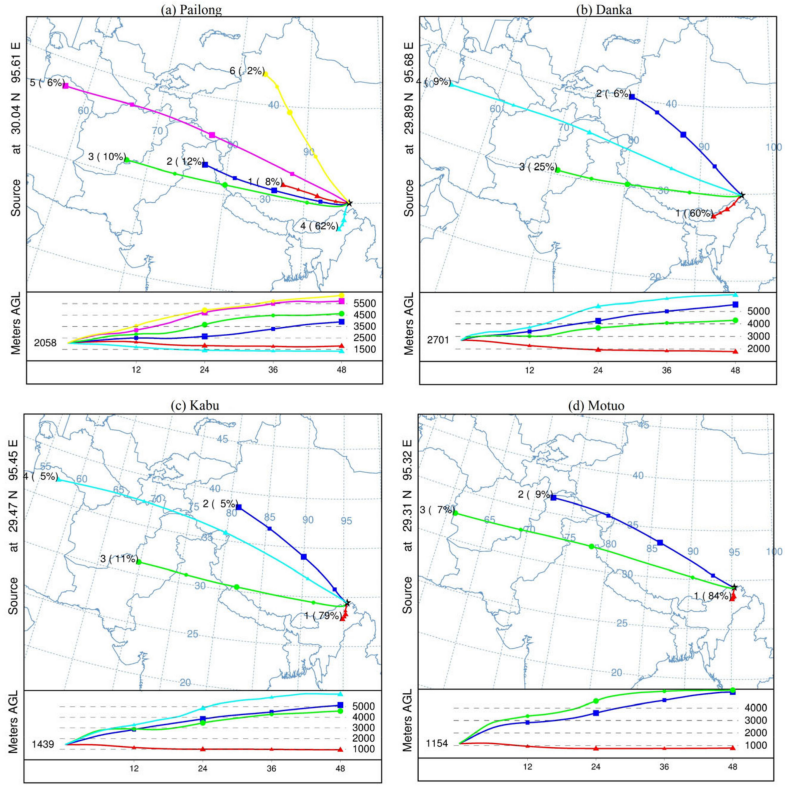

Figure 9. The same as Figure 7 but for each station in autumn. (**a**) Pailong station, (**b**) Danka station, (**c**) Kabu station, (**d**) Motuo station.

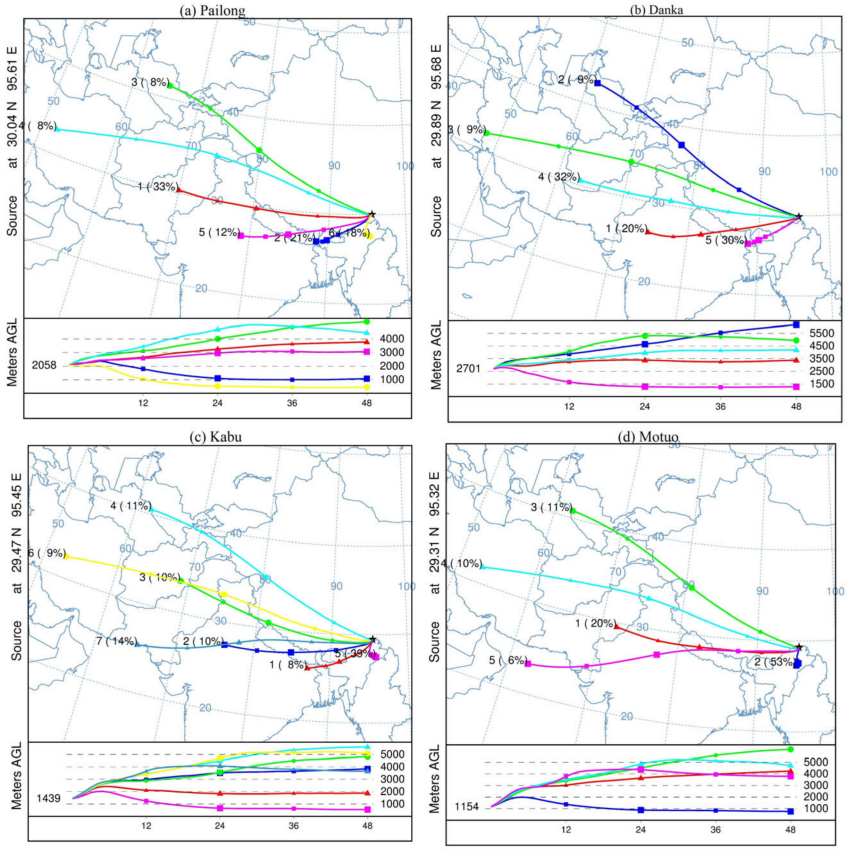

Figure 10. The same as Figure 7 but for each station in winter. (**a**) Pailong station, (**b**) Danka station, (**c**) Kabu station, (**d**) Motuo station.

4.6. Vertical Characteristics of Water Vapor Exchange between Upper Troposphere and Lower Stratosphere

Recent study has verified that the TP is a water vapor convergence area from horizontal point of view, where the convergence was enhanced from 1979 to 2018 [46]. However, the vertical characteristics of water vapor exchange between upper troposphere and lower stratosphere (UTLS) is still unclear so far. Therefore, the climatological distribution of UTLS water vapor exchange over the TP was estimated using ERA5 reanalysis data (1979–2018) with the model proposed by [60]. It can be found that troposphere to stratosphere transport (TST) dominated over the central TP in spring, while stratosphere to troposphere transport (STT) played a major role over the western TP and the eastern TP (Figure 11a). In summer, the absolute high value centers of TST moved northeastward, and the original absolute high value centers of STT in spring over the TP were inverted from downwelling to upwelling, leaving the whole TP dominated by TST (Figure 11b). In autumn, the spatiotemporal distribution pattern of vertical water vapor exchange was similar to that in spring, while exhibiting relatively weaker exchange intensity (Figure 11c). In winter, most areas were all dominated by STT, with the eastern region and the western frontier as the absolute high value zones (Figure 11d). The spatial distribution characteristic of vertical water vapor exchange over the TP may result from the combinational effects of the thermal forcing of the TP, the mechanical forcing of the large-scale topography and the vertical discontinuity of tropopause and tropopause pressure. The horizontal transport term, the vertical transport term and the transport term due to the variability of tropopause of the UTLS water vapor exchange over the TP were calculated, respectively. The results show that both the horizontal and vertical transport term made main contribution to the total water vapor exchange, while the water vapor exchange due to tropopause variation was minor. From the perspective of seasonal variability, these three terms exhibited significant

differences between winter and summer, while the spatial pattern of the UTLS water vapor exchange was closest to that of the vertical transport term.

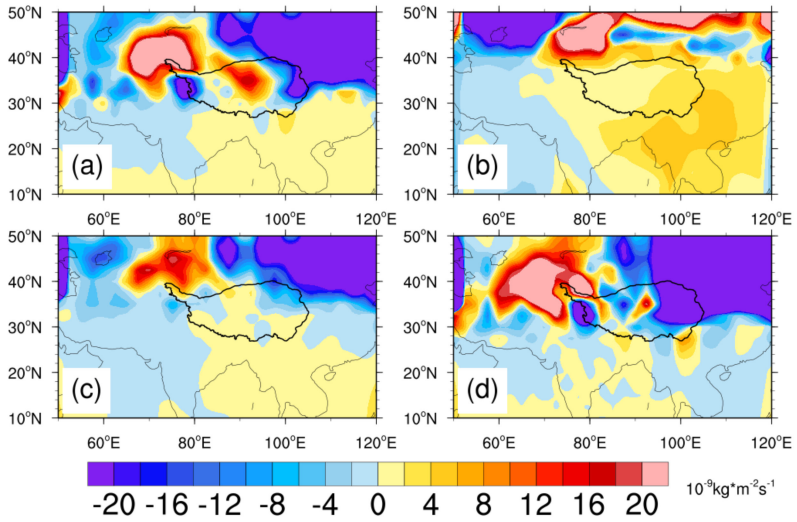

Figure 11. The troposphere–stratosphere water vapor exchange over the TP (1979–2018): (**a**) spring, (**b**) summer, (**c**) autumn and (**d**) winter. (Positive values indicate upward water vapor transport).

5. Discussion and Conclusions

Climate change will likely affect the Asian water towers [61], but current climate projections do not adequately reproduce past and current climate in TPE and are inadequate to assess impacts on water resources and agriculture [62]. It had been previously reported that many remote sensing products of soil moisture did not compare favourably with in situ observation on the Tibetan plateau [11,18], and the most advanced ECMWF modelling system also has difficulty in reproducing the observed soil moisture and soil temperature profiles on the Tibetan plateau [11]. The new analysis based on the Tibet-Obs data also confirm these findings for the improved products (e.g., ERA5, see Section 4.4). The CLIMATE-TPE project has contributed to a reduction in these uncertainties by introducing process for understanding the whole TPE into observation models, which has been shown to be feasible on a local scale by [12–14,21–23,63]. The extension of these understandings to the whole TPE needs to be pursued in future.

Based on the Tibet-Obs, it has been possible to produce improved plateau scale merged surface soil moisture products [33] and root zone soil moisture [34]. These plateau scale data are also invaluable for improving retrieval algorithms used in current operations (e.g., [64–66]) and the importance in observing processes has been demonstrated (e.g., consideration of the dielectric roughness of the surface) for the successful simulation of the observed brightness temperature [29]. The collected data have also been used to develop retrieval methods for the physical properties of soil via assimilating satellite brightness temperature observations [19,26]. Progress has also been made in understanding the mass, momentum and energy transfer in the frozen soil and the freezing–thawing processes [21,22]. It has also been shown that the inclusion of the freezing–thawing processes is important for the correct modeling of ecosystem dynamics [63]. Modelling of the ecosystems in TP at climate scale needs to be conducted to investigate the significance of freezing–thawing processes in explaining the observed changes and improving predictions of future changes and helping to devise adaptation and mitigation measures.

The novel characters of the CLIMATE-TPE project to science can be summarised as (1) An advancement of the understanding of microwave scattering and emission under complex terrains, including permafrost and freezing and thawing; future works are needed to extend the current understanding to multi-frequency satellite observations. This will enable the analysis of past satellite microwave observations of the pan TPE areas. (2) An advancement of the physical understanding and quantification of changes in water and

energy budgets in TPE. These quantifications should be conducted for the different energy and water budget terms given in Equations (1)–(5) and be linked to satellite observation of the changes in vegetation and ecosystems. (3) An advancement in quantifying the changes in surface characteristics and monsoon interactions. While we have succeeded in analyzing and explaining the different surface characteristics, a unified analysis of all related surface features and monsoon interactions may provide a deeper understanding of the climatic connections of these different aspects. Since the TPE region has gained growing attention due to its significant role in global atmospheric circulation and its sensitivity in providing a first indication of climate changes, a fundamental understating of this region's natural environment is also vital for a better understanding of global climate changes and interactions with human activities. Consolidated data records of essential water variables need to be generated for climate analysis and for model validation by combining in situ data, satellite observations and numerical modelling.

The key societal contribution of the CLIMATE-TPE project is to quantify the status and fate of water resources in TPE so that the planning and management of the vital water resources for 1.5 billion people across 10 countries in the TPE can be based on quantitative data and information. The CLIMATE-TPE project primarily focused on the observation, explanation and modeling of physical processes in land–atmosphere interactions and impacts of climate change in TPE. It would be interesting to compare the findings of the CLIMATE-TPE project to those of other initiatives such as the Changing Cold Regions Network (CCRN) [67,68] and investigate climate change adaptation and mitigation measures in future research.

The CLIMATE-TPE project has contributed to the objectives of the Dragon 4 programme in the following programmatic aspects:

(1) Promote the exploitation of ESA and Chinese EO data for science and application development with an emphasis on generating climate data records related to essential water variables using ESA and Chinese EO data;
(2) Stimulate scientific exchanges by forming joint Sino-European teams by means of academic exchanges, in particular of young scientists. This was an extension of the Dragon 3 programme and other collaborative projects;
(3) Provide training to young European and Chinese scientists. We have continued the successful joint supervision of young scientists started from Dragon 1, 2, 3 programme, and so far there have been 17 joint PhD promotions (Dr. R. van der Velde, Dr. J. Timmermans, Dr. C. Qin, Dr. Y. Zeng, Dr. X. Chen, Dr. L. Zhong, Dr. J. Malik, Dr. X. Tian, Dr. L. Li, Dr. D. Zheng, Dr. Y. Huang, Dr. L. Dente, Dr. B. Wang, Dr. S. Lv, Dr. Q. Wang, Dr. X. Yuan, Dr. H. Zhao and several ongoing PhD researchers (a list can be found at https://www.itc.nl/research/phd-projects/?researchtheme=wcc) (accessed on 6 September 2021);
(4) Publish co-authored results in ESA-NRSCC joint results publication and in leading scientific journals. A list of publications resulted in partial support by previous Dragon programme can be found in Appendix A).

Based on the obtained results and the unsolved challenges reported in this paper, we propose that future research should focus on the following outstanding scientific questions:

(1) While progress has been made to estimate the various water and energy budgets terms in Equations (1)–(3), their degree of closure and climatic consistencies have not been assessed in the TPE. Does the TPE have a more accelerated water cycle (i.e., fluxes) and water cycle dynamics (i.e., stores) than other regions in the world? To address this question, we need to independently quantify the different terms of water store and flux terms in Equations (1)–(3). Current and future satellite observations, together with numerical modeling, can help to advance this science issue by quantifying the amount of moisture stores at and below the land surface as soil moisture and surface water store and groundwater, respectively, and precipitation and evaporation, while more in situ observations are needed to quantify the net surface and groundwater runoff. Examples of this are the hydrological and geophysical investigations currently

conducted in the Maqu catchment. The quantification of these water and energy budgets need to extend to climate scale.

(2) What is the impact of and feedback to the Asian monsoon and the westerlies systems of the TPE's water and energy budget? Because the precipitation and evaporation balance the atmospheric water vapor storage and horizontal convergence on the one hand and control the increase of water storage on land and runoff, analyzing these terms consistently with Equations (4) and (5) could help in detecting impacts and feedback between TPE and changes in the external monsoon and westerlies. These analyses need to be conducted in conjunction with analysis of the dynamics of the boundary layer dynamics and the interactions between the upper troposphere and lower stratosphere of the Tibetan atmosphere. This will provide the much-needed insights regarding the impact of climate change impact in TPE.

(3) Given the projected global warming, what would be the consequences to the water resource availability in TPE and what adaptation and mitigation measures could be devised for policy making? This framework in (1) and (2) above, i.e., Equations (1)–(5), can be integrated into a regional Earth system model of the TPE and long-term simulations can be conducted to examine different scenarios.

Because the TPE is a data-scarce region regarding the various water and energy balance terms in Equations (1)–(5), we propose future research to emphasize on the following areas:

(4) What are the mechanisms and controls of the different land surface processes, heavy precipitation, ponding surface water, snow and snowmelt, frozen ground, freeze-thaw, permafrost and different ecosystem and landscape forms on the satellite signals of microwave scattering and emission? Integration of the observation operator (i.e., a forward signal simulator to simulate satellite observation) into an Earth system model (ESM) may help to overcome these challenges.

(5) Can the changes of water and energy budgets in the TPE be simulated with current land surface and integrated models as used in current reanalysis? This issue may be addressed by first analyzing the consistency of available data records from satellite observations and reanalysis and gradually improving the process description in the ESM to reflect what is observed by satellite observation. This would advance the development of a more adequate ESM for the TPE.

There are currently still many unexplained uncertainties in current microwave satellite observations over complex terrain and inaccuracies in retrievals of soil moisture and freeze–thaw states. By deploying in situ observations, laboratory experiments and numerical modelling with the obtained datasets, these uncertainties and inaccuracies can be largely reduced, and capabilities can be developed to utilize the current and future satellite observations of TPE. These advanced process understandings can be integrated into observation operator models that can be used to simulate and explain satellite observation signals from optical, thermal and microwave spectra. When these models are coupled with process models of energy, water and CO_2 fluxes, consistent climate data records on energy, water and carbon cycles of TPE can be generated. These datasets would be invaluable to reveal the impacts of climate change and help to propose adaptation and mitigation measures. Systematic analysis can be made of all variables related to water, energy and carbon budgets in TPE to ensure their consistency in terms of climate data records. These variables may include albedo, vegetation coverage, soil thermal and hydraulic properties, land surface temperature, soil moisture, lake levels and land use changes, among others, that can be retrieved from satellite observations. When the observation operators, the process models and long-term climate data records can be integrated into Earth system models, climate change impacts on water resources and ecosystems can be modelled and projections for future changes made.

Author Contributions: Conceptualization, Z.S., Y.M., J.S., M.J.P., J.W., Y.H. and X.D.; investigation, all authors; writing—original draft preparation, Z.S.; writing—review and editing, all authors. All authors have read and agreed to the published version of the manuscript.

Funding: This work was supported in part by the ESA MOST Dragon IV Program (project: Monitoring Water and Energy Cycles at Climate Scale in the Third Pole Environment), ESA ELBARA-II/III Loan Agreement EOP-SM/2895/TC-tc, the Netherlands Organization for Scientific Research under Project ALW-GO/14-29, the Netherlands eScience Center under project ASDI.2020.026, the National Natural Science Foundation of China (grant no. 91837208, 41971033, 41675106) and the Fundamental Research Funds for the Central Universities, CHD (grant no. 300102298307).

Institutional Review Board Statement: Not applicable.

Informed Consent Statement: Not applicable.

Data Availability Statement: The data cited in this paper can be accessed at: https://data.tpdc.ac.cn/en/data/a08ac15d-06a1-4150-806c-50b8d8b0f72a/?q=soil%20moisture and https://ismn.geo.tuwien.ac.at/en/ (accessed on 6 September 2021, *Tibet-Obs soil moisture and soil temperature*); https://doi.org/10.6084/m9.figshare.12728444.v1 (accessed on 6 September 2021, *in-situ L-band microwave radiometry*); https://doi.org/10.17026/dans-zc5-skyg (accessed on 6 September 2021, *Long-term ground-based broadband microwave scatterometer observations of an alpine meadow over the Tibetan Plateau*); https://data.tpdc.ac.cn/en/data/df4005fb-9449-4760-8e8a-09727df9fe36/?q=evapotranspiration (accessed on 6 September 2021, *Surface energy balance based global land evapotranspiration*); https://data.tpdc.ac.cn/en/data/5a0d2e28-ebc6-4ea4-8ce4-a7f2897c8ee6/?q=evapotranspiration (accessed on 6 September 2021, *Monthly mean evapotranspiration data set of the Tibetan Plateau (2001–2018)*).

Acknowledgments: We thank the Zoige Plateau Wetlands Ecosystem Research Station, Northwest Institute of Eco-Environment and Resources, Chinese Academy of Science, Lanzhou, China, for providing precipitation data from 1 September 2016 to 30 January 2017, and we are grateful to colleagues and institutions who have supported our field experiment and campaigns.

Conflicts of Interest: The authors declare no conflict of interest.

Abbreviations

AATSR	the Advanced Along Track Scanning Radiometer
AGL	height Above Ground Level
AIEM	advanced integral equation model
ALOS	Advanced Land Observing Satellite
AMSRE-E/2	Advanced Microwave Scanning Radiometer (AMSR)
AQUA	Aqua is a NASA scientific research satellite in orbit around the Earth
ASAR	the Advanced Synthetic Aperture Radar
ATS	an air-to-soil dielectric transition model
CAREERI	Cold and Arid Regions Environmental Engineering Research Institute
CAS	Chinese Academy of Sciences
CCI	climate change initiative
CDR/ECV	climate data record, essential climate variable
CMA	China Meteorological Administration
CMEM	community microwave emission modelling platform
CMIP6	Coupled Model Intercomparison Project
CNMC	China National Meteorological Centre
CO_2/H_2O	carbon dioxide and water
CORE-CLIMAX	the project for COordinating Earth observation data validation for RE-analysis for CLIMAte ServiceS
COSMIC	The COsmic-ray Soil Moisture Interaction Code
ECMWF	European Centre for Medium-Range Weather Forecasts
ELBARA-III	ESA L-Band Radiometer, 3rd Generation
ENVISAT	Environmental Satellite
EO	Earth Observation
ERA-interim	The ECMWF interim reanalysis covering the period from 1979 onwards
ERS	European Remote Sensing satellite
ESA	European Space Agency
ET	Evapotranspiration

FY	Fengyun referring to China's weather satellites
GLDAS	the Global Land Data Assimilation System
GLEAM	Global Land Evaporation Amsterdam Model
ITP	Institute of Tibetan Plateau Research
LAI	leaf area index
LST	land surface temperature
MERIS	MEdium Resolution Imaging Spectrometer (MERIS)
MOD16	MODIS global evapotranspiration product
MODIS	Moderate Resolution Imaging Spectroradiometer
NASA	The National Aeronautics and Space Administration
NCAR	National Center for Atmospheric Research
NCEP	National Centers for Environmental Prediction
SCAT/ASCAT	scatterometer and advanced scatterometer
SEBS	Surface Energy Balance System
SMAP	Soil Moisture Active Passive
SMOS	Soil Moisture and Ocean Salinity satellite
SSM/I	the Special Sensor Microwave/Imager
STEMMUS-FT	Simultaneous Transfer of Energy, Mass, and Momentum in Unsaturated Soils with Freeze–Thaw
STT	stratosphere to troposphere transport
TERRA	a multi-national NASA scientific research satellite
TPE	Third Pole Environment
TPM	Third Party Mission, referring to Third Party satellite Mission
TST	troposphere to stratosphere transport
TVG	a discrete scattering-emission model for vegetation (known also as the Tor Vergata model)
UTLS	upper troposphere and lower stratosphere
VISSR	multi-channel Visible and Infrared Spin Scan Radiometer
WGS'84	The World Geodetic System 1984
WRF	the Weather Research and Forecasting (*WRF*) *Model*

Appendix A. List of Publications in Dragon 4 CLIMATE-TPE Project

(1) J. P. Ngarukiyimana, Y. Fu, C. Sindikubwabo, I. F. Nkurunziza, F. K. Ogou, F. Vuguziga, B. A. Ogwang, and Y. Yang, "Climate Change in Rwanda: The Observed Changes in Daily Maximum and Minimum Surface Air Temperatures during 1961–2014," Frontiers in Earth Science, vol. 9, p. 106, 2021, doi:10.3389/feart.2021.619512.

(2) Y. Wang, Z. Zhu, Y. Ma, and L. Yuan, "Carbon and water fluxes in an alpine steppe ecosystem in the Nam Co area of the Tibetan Plateau during two years with contrasting amounts of precipitation," International Journal of Biometeorology, vol. 64, pp. 1183–1196, 2020.

(3) V. K. Oad, X. Dong, M. Arfan, V. Kumar, M. S. Mohsin, S. Saad, H. Lu, M. I. Azam, and M. Tayyab, "Identification of Shift in Sowing and Harvesting Dates of Rice Crop (L. Oryza sativa) through Remote Sensing Techniques: A Case Study of Larkana District," Sustainability, vol. 12, n. 3586, 2020, doi:10.3390/su12093586.

(4) S. Luo, Y. Fu, S. Zhou, X. Wang, and D. Wang, "Analysis of the Relationship between the Cloud Water Path and Precipitation Intensity of Mature Typhoons in the Northwest Pacific Ocean," Advances in Atmospheric Sciences, vol. 37, pp. 359–376, 2020.

(5) M. Waseem, I. Ahmad, A. Mujtaba, M. Tayyab, C. Si, H. Lue, and X. Dong, "Spatiotemporal Dynamics of Precipitation in Southwest Arid-Agriculture Zones of Pakistan," Sustainability, vol. 12, n. 2305, 2020, doi:10.3390/su12062305.

(6) Y. Fu, Y. Ma, L. Zhong, Y. Yang, X. Guo, C. Wang, X. Xu, K. Yang, X. Xu, L. Liu, G. Fan, Y. Li, and D. Wang, "Land-surface processes and summer-cloud-precipitation

characteristics in the Tibetan Plateau and their effects on downstream weather: a review and perspective," National Science Review, vol. 7, pp. 500–515, 2020.
(7) K. Xu, L. Zhong, Y. Ma, M. Zou, and Z. Huang, "A study on the water vapor transport trend and water vapor source of the Tibetan Plateau," Theoretical and Applied Climatology, vol. 140, pp. 1031–1042, 2020.
(8) L. Yu, Y. Fu, Y. Yang, X. Pan, and R. Tan, "Trumpet-Shaped Topography Modulation of the Frequency, Vertical Structures, and Water Path of Cloud Systems in the Summertime Over the Southeastern Tibetan Plateau: A Perspective of Daytime-Nighttime Differences," Journal of Geophysical Research, vol. 125, no. 3, n. e2019JD031803, 2020, doi:10.1029/2019JD031803.
(9) N. Ge, L. Zhong, Y. Ma, M. Cheng, X. Wang, M. Zou, and Z. Huang, "Estimation of Land Surface Heat Fluxes Based on Landsat 7 ETM+ Data and Field Measurements over the Northern Tibetan Plateau," Remote Sensing, vol. 11, n. 2899, 2019, doi:10.3390/rs11242899.
(10) F. Chen, W. T. Crow, M. H. Cosh, A. Colliander, J. Asanuma, A. Berg, D. D. Bosch, T. G. Caldwell, C. H. Collins, K. H. Jensen, J. Martinez-Fernandez, H. McNairn, P. J. Starks, Z. Su, and J. P. Walker, "Uncertainty of Reference Pixel Soil Moisture Averages Sampled at SMAP Core Validation Sites," Journal of Hydrometeorology, vol. 20, pp. 1553–1569, 2019.
(11) L. Zhong, Y. Ma, Y. Xue, and S. Piao, "Climate Change Trends and Impacts on Vegetation Greening Over the Tibetan Plateau," Journal of Geophysical Research, vol. 124, pp. 7540–7552, 2019.
(12) B. Wang, Y. Ma, Y. Wang, Z. Su, and W. Ma, "Significant differences exist in lake-atmosphere interactions and the evaporation rates of high-elevation small and large lakes," Journal of Hydrology, vol. 573, pp. 220–234, 2019.
(13) L. Zhong, K. Xu, Y. Ma, Z. Huang, X. Wang, and N. Ge, "Evapotranspiration Estimation Using Surface Energy Balance System Model: A Case Study in the Nagqu River Basin," Atmosphere vol. 10, n. 268, 2019, doi:10.3390/atmos10050268.
(14) Z. Wei, Y. Meng, W. Zhang, J. Peng, and L. Meng, "Downscaling SMAP soil moisture estimation with gradient boosting decision tree regression over the Tibetan Plateau," Remote Sensing of Environment, vol. 225, pp. 30–44, 2019.
(15) B. Wang, Y. Ma, W. Ma, B. Su, and X. Dong, "Evaluation of ten methods for estimating evaporation in a small high-elevation lake on the Tibetan Plateau," Theoretical and Applied Climatology, vol. 136, pp. 1033–1045, 2019.
(16) Q. Wang, R. van der Velde, P. Ferrazzoli, X. Chen, X. Bai, and Z. Su, "Mapping soil moisture across the Tibetan Plateau plains using Aquarius active and passive L-band microwave observations," International Journal of Applied Earth Observation and Geoinformation, vol. 77, pp. 108–118, 2019.
(17) L. Zhong, Y. Ma, Z. Hu, Y. Fu, Y. Hu, X. Wang, M. Cheng, and N. Ge, "Estimation of hourly land surface heat fluxes over the Tibetan Plateau by the combined use of geostationary and polar-orbiting satellites," Atmospheric Chemistry and Physics, vol. 19, pp. 5529–5541, 2019.
(18) M. Zou, L. Zhong, Y. Ma, Y. Hu, and L. Feng, "Estimation of actual evapotranspiration in the Nagqu river basin of the Tibetan Plateau," Theoretical and Applied Climatology, vol. 132, pp. 1039–1047, 2018.
(19) M. Zou, L. Zhong, Y. Ma, Y. Hu, Z. Huang, K. Xu, and L. Feng, "Comparison of Two Satellite-Based Evapotranspiration Models of the Nagqu River Basin of the Tibetan Plateau," Journal of Geophysical Research, vol. 123, pp. 3961–3975, 2018.
(20) Y. Hu, L. Zhong, Y. Ma, M. Zou, K. Xu, Z. Huang, and L. Feng, "Estimation of the Land Surface Temperature over the Tibetan Plateau by Using Chinese FY-2C Geostationary Satellite Data," Sensors, vol. 18, n. 376, 2018, doi:10.3390/s18020376.
(21) M. Cheng, L. Zhong, Y. Ma, M. Zou, N. Ge, X. Wang, and Y. Hu, "A study on the assessment of multi-source satellite soil moisture products and reanalysis data for the Tibetan Plateau," Remote Sensing, vol. 11, n. 1196, 2019, doi:10.3390/rs11101196.

(22) S. Lv, Y. Zeng, J. Wen, H. Zhao, and Z. Su, "Estimation of penetration depth from soil effective temperature in microwave radiometry," Remote Sensing, vol. 10, n. 519, 2018, doi:10.3390/rs10040519.

References

1. He, H.; McGinnis, J.W.; Song, Z.; Yanai, M. Onset of the Asian summer monsoon in 1979 and the effect of the Tibetan Plateau. *Mon. Weather Rev.* **1987**, *115*, 1966–1995. [CrossRef]
2. Ueda, H.; Yasunari, T. Role of warming over the Tibetan Platean in early onset of the summer monsoon over the bay of Bengal and the South China Sea. *J. Meteorol. Soc. Jpn.* **1998**, *76*, 1–12. [CrossRef]
3. Wu, G.; Zhang, Z. Tibetan Plateau forcing and the timing of the monsoon onset over South Asia and the South China Sea. *Mon. Weather Rev.* **1998**, *126*, 913–927. [CrossRef]
4. Yanai, M.; Li, C.; Song, Z. Seasonal heating of the Tibetan Plateau and its effects on the evolution of the Asian summer monsoon. *J. Meteorol. Soc. Jpn.* **1992**, *70*, 319–351. [CrossRef]
5. Yanai, M.; Li, C. Mechanism of heating and the boundary layer over the Tibetan Plateau. *Mon. Weather Rev.* **1994**, *122*, 305–323. [CrossRef]
6. Wu, T.-W.; Qian, Z.-A. The relation between the Tibetan winter snow and the Asian summer monsoon and rainfall: An observational investigation. *J. Clin.* **2003**, *16*, 2038–2051. [CrossRef]
7. Zhang, Y.; Li, T.; Wang, B. Decadal change of the spring snow depth over the Tibetan Plateau: The associated circulation and influence on the east Asian summer monsoon. *J. Clim.* **2004**, *17*, 2780–2793. [CrossRef]
8. Boos, W.R.; Kuang, Z. Dominant control of the South Asian monsoon by orographic insulation versus plateau heating. *Nature* **2010**, *463*, 218–222. [CrossRef]
9. Wu, G.; Liu, Y.; He, B.; Bao, Q.; Duan, A.; Jin, F.F. Thermal controls on the Asian summer monsoon. *Sci. Rep.* **2012**, *2*, 404. [CrossRef]
10. Su, Z.; Wen, J.; Dente, L.; van der Velde, R.; Wang, L.; Ma, Y.; Yang, K.; Hu, Z. The Tibetan Plateau observatory of plateau scale soil moisture and soil temperature (Tibet-Obs) for quantifying uncertainties in coarse resolution satellite and model products. *Hydrol. Earth Syst. Sci.* **2011**, *15*, 2303–2316. [CrossRef]
11. Su, Z.; De Rosnay, P.; Wen, J.; Wang, L.; Zeng, Y. Evaluation of ECMWF's soil moisture analyses using observations on the Tibetan Plateau. *J. Geophys. Res. Atmos.* **2013**, *118*, 5304–5318. [CrossRef]
12. Zheng, D.; van der Velde, R.; Su, Z.; Wang, X.; Wen, J.; Booij, M.J.; Hoekstra, A.; Chen, Y. Augmentations to the Noah model physics for application to the Yellow River source area. Part I: Soil water flow. *J. Hydrometeorol.* **2015**, *16*, 2659–2676. [CrossRef]
13. Zheng, D.; Van Der Velde, R.; Su, Z.; Wang, X.; Wen, J.; Booij, M.J.; Hoekstra, A.Y.; Chen, Y. Augmentations to the Noah model physics for application to the Yellow River source area. Part II: Turbulent heat fluxes and soil heat transport. *J. Hydrometeorol.* **2015**, *16*, 2677–2694. [CrossRef]
14. Zheng, D.; Van Der Velde, R.; Su, Z.; Booij, M.J.; Hoekstra, A.Y.; Wen, J. Assessment of roughness length schemes implemented within the Noah land surface model for high-altitude regions. *J. Hydrometeorol.* **2014**, *15*, 921–937. [CrossRef]
15. Schwank, M.; Wiesmann, A.; Werner, C.; Mätzler, C.; Weber, D.; Murk, A.; Völksch, I.; Wegmüller, U. ELBARA II, an L-band radiometer system for soil moisture research. *Sensors* **2010**, *10*, 584–612. [CrossRef]
16. Su, Z.; Wen, J.; Zeng, Y.; Zhao, H.; Lv, S.; Van Der Velde, R.; Zheng, D.; Wang, X.; Wang, Z.; Schwank, M.; et al. Multiyear in-situ L-band microwave radiometry of land surface processes on the Tibetan Plateau. *Sci. Data* **2020**, *7*, 1–13. [CrossRef]
17. Lv, S.; Wen, J.; Zeng, Y.; Tian, H.; Su, Z. An improved two-layer algorithm for estimating effective soil temperature in microwave radiometry using in situ temperature and soil moisture measurements. *Remote Sens. Environ.* **2014**, *152*, 356–363. [CrossRef]
18. Dente, L.; Ferrazzoli, P.; Su, Z.; van Der Velde, R.; Guerriero, L. Combined use of active and passive microwave satellite data to constrain a discrete scattering model. *Remote Sens. Environ.* **2014**, *155*, 222–238. [CrossRef]
19. Zhao, H.; Zeng, Y.; Han, X.; Su, Z. Retrieving Soil Physical Properties via Assimilating SMAP Brightness Temperature Observations in the Community Land Model. *J. Adv. Modell. Earth Syst.* **2021**. in review.
20. Wang, B.; Ma, Y.; Wang, Y.; Su, Z.; Ma, W. Significant differences exist in lake-atmosphere interactions and the evaporation rates of high-elevation small and large lakes. *J. Hydrol.* **2019**, *573*, 220–234. [CrossRef]
21. Yu, L.; Zeng, Y.; Su, Z. Understanding the mass, momentum, and energy transfer in the frozen soil with three levels of model complexities. *Hydrol. Earth Syst. Sci.* **2020**, *24*, 4813–4830. [CrossRef]
22. Yu, L.; Zeng, Y.; Wen, J.; Su, Z. Liquid-Vapor-Air Flow in the Frozen Soil. *J. Geophys. Res. Atmos.* **2018**, 7393–7415. [CrossRef]
23. Mwangi, S.; Zeng, Y.; Montzka, C.; Yu, L.; Su, Z. Assimilation of cosmic-ray neutron counts for the estimation of soil ice content on the eastern Tibetan Plateau. *J. Geophys. Res. Atmos.* **2020**, *125*, 1–23. [CrossRef]
24. Zeng, Y.; Su, Z.; Barmpadimos, I.; Perrels, A.; Poli, P.; Boersma, K.F.; Frey, A.; Ma, X.; de Bruin, K.; Goosen, H.; et al. Towards a traceable climate service: Assessment of quality and usability of essential climate variables. *Remote Sens.* **2019**, *11*, 1186. [CrossRef]
25. Zeng, Y.; Su, Z.; Calvet, J.-C.; Manninen, T.; Swinnen, E.; Schulz, J.; Roebeling, R.; Poli, P.; Tan, D.; Riihelä, A.; et al. Analysis of current validation practices in Europe for space-based climate data records of essential climate variables. *Int. J. Appl. Earth Obs. Geoinf.* **2015**, *42*, 150–161. [CrossRef]
26. Zhao, H.; Zeng, Y.; Lv, S.; Su, Z. Analysis of soil hydraulic and thermal properties for land surface modeling over the Tibetan Plateau. *Earth Syst. Sci. Data* **2018**, *10*, 1031–1061. [CrossRef]

27. Lv, S.; Zeng, Y.; Su, Z.; Wen, J. A Closed-Form Expression of Soil Temperature Sensing Depth at L-Band. *IEEE Trans. Geosci. Remote Sens.* **2019**, *57*, 4889–4897. [CrossRef]
28. Hofste, J.G.; van der Velde, R.; Wen, J.; Wang, X.; Wang, Z.; Zheng, D.; van der Tol, C.; Su, Z. Year-long, broad-band, microwave backscatter observations of an alpine meadow over the Tibetan Plateau with a ground-based scatterometer. *Earth Syst. Sci. Data* **2021**, *13*, 2819–2856. [CrossRef]
29. Zhao, H.; Zeng, Y.; Wen, J.; Wang, X.; Wang, Z.; Meng, X.; Su, Z. An Air-to-Soil Transition Model for Discrete Scattering-Emission Modelling at L-Band. *J. Remote Sens.* **2021**, *2021*, 1–20. [CrossRef]
30. Zheng, D.; Li, X.; Wang, X.; Wang, Z.; Wen, J.; van der Velde, R.; Schwank, M.; Su, Z. Sampling depth of L-band radiometer measurements of soil moisture and freeze-thaw dynamics on the Tibetan Plateau. *Remote Sens. Environ.* **2019**, *226*, 16–25. [CrossRef]
31. Wang, B.; Ma, Y.; Su, Z.; Wang, Y.; Ma, W. Quantifying the evaporation amounts of 75 high-elevation large dimictic lakes on the Tibetan Plateau. *Sci. Adv.* **2020**, *6*, eaay8558. [CrossRef]
32. Wei, Z.; Meng, Y.; Zhang, W.; Peng, J.; Meng, L. Downscaling SMAP soil moisture estimation with gradient boosting decision tree regression over the Tibetan Plateau. *Remote Sens. Environ.* **2019**, *225*, 30–44. [CrossRef]
33. Zeng, Y.; Su, Z.; van der Velde, R.; Wang, L.; Xu, K.; Wang, X.; Wen, J. Blending Satellite Observed, Model Simulated, and in Situ Measured Soil Moisture over Tibetan Plateau. *Remote Sens.* **2016**, *8*, 268. [CrossRef]
34. Zhuang, R.; Zeng, Y.; Manfreda, S.; Su, Z. Quantifying Long-Term Land Surface and Root Zone Soil Moisture over Tibetan Plateau. *Remote Sens.* **2020**, *12*, 509. [CrossRef]
35. Chen, X.; Su, Z.; Ma, Y.; Middleton, E.M. Optimization of a remote sensing energy balance method over different canopy applied at global scale. *Agric. Forest Meteorol.* **2019**, *279*. [CrossRef]
36. Zhong, L.; Ma, Y.; Hu, Z.; Fu, Y.; Hu, Y.; Wang, X.; Cheng, M.; Ge, N. Estimation of hourly land surface heat fluxes over the Tibetan Plateau by the combined use of geostationary and polar-orbiting satellites. *Atmospheric Chem. Phys.* **2019**, *19*, 5529–5541. [CrossRef]
37. Cheng, M.; Zhong, L.; Ma, Y.; Zou, M.; Ge, N.; Wang, X.; Hu, Y. A Study on the Assessment of Multi-Source Satellite Soil Moisture Products and Reanalysis Data for the Tibetan Plateau. *Remote Sens.* **2019**, *11*, 1196. [CrossRef]
38. Zhong, L.; Huang, Z.; Ma, Y.; Fu, Y.; Chen, M.; Ma, M.; Zheng, J. Assessments of Weather Research and Forecasting Land Surface Models in Precipitation Simulation Over the Tibetan Plateau. *Earth Space Sci.* **2021**, *8*. [CrossRef]
39. Ma, Y.; Hu, Z.; Xie, Z.; Ma, W.; Wang, B.; Chen, X.; Li, M.; Zhong, L.; Sun, F.; Gu, L.; et al. A long-term (2005-2016) dataset of hourly integrated land-atmosphere interaction observations on the Tibetan Plateau. *Earth Syst. Sci. Data* **2020**, *12*, 2937–2957. [CrossRef]
40. Ma, Y.; Ma, W.; Zhong, L.; Hu, Z.; Li, M.; Zhu, Z.; Han, C.; Wang, B.; Liu, X. Monitoring and Modeling the Tibetan Plateau's climate system and its impact on East Asia. *Sci. Rep.* **2017**, *7*. [CrossRef]
41. Lv, S.; Simmer, C.; Zeng, Y.; Su, Z.; Wen, J. L-band Microwave Emission of Frozen Soil during the Thawing Period. *Remote Sens. Environ.* **2021**. in review.
42. Fung, A.K.; Li, Z.Q.; Chen, K.S. Backscattering from a randomly rough dielectric surface. *IEEE Trans. Geosci. Remote Sens.* **1992**, *30*, 356–369. [CrossRef]
43. Chen, K.S.; Wu, T.D.; Tsang, L.; Li, Q.; Shi, J.C.; Fung, A.K. Emission of rough surfaces calculated by the integral equation method with comparison to three-dimensional moment method Simulations. *IEEE Trans. Geosci. Remote Sens.* **2003**, *41*, 90–101. [CrossRef]
44. Ferrazzoli, P.; Guerriero, L. Passive microwave remote sensing of forests: A model investigation. *IEEE Trans. Geosci. Remote Sens.* **1996**, *34*, 433–443. [CrossRef]
45. Wang, Z.; Zhan, C.; Ning, L.; Guo, H. Evaluation of global terrestrial evapotranspiration in CMIP6 models. *Theoretical Appl. Climatol.* **2021**, *143*, 521–531. [CrossRef]
46. Zhu, Z.; Piao, S.; Myneni, R.B.; Huang, M.; Zeng, Z.; Canadell, J.G.; Ciais, P.; Sitch, S.; Friedlingstein, P.; Arneth, A.; et al. Greening of the Earth and its drivers. *Nat. Climate Change* **2016**, *6*, 791. [CrossRef]
47. Chen, X.; Su, Z.; Ma, Y.; Yang, K.; Wen, J.; Zhang, Y. An Improvement of Roughness Height Parameterization of the Surface Energy Balance System (SEBS) over the Tibetan Plateau. *J. Appl. Meteorol. Climatol.* **2013**, *52*, 607–622. [CrossRef]
48. Su, Z. The Surface Energy Balance System(SEBS) for estimation of turbulent heat fluxes. *Hydrol. Earth Syst. Sci.* **2002**, *6*, 85–99. [CrossRef]
49. Mu, Q.; Zhao, M.; Running, S.W. Improvements to a MODIS global terrestrial evapotranspiration algorithm. *Remote Sens. Environ.* **2011**, *115*, 1781–1800. [CrossRef]
50. Martens, B.; Miralles, D.G.; Lievens, H.; van der Schalie, R.; de Jeu, R.A.M.; Fernández-Prieto, D.; Beck, H.E.; Dorigo, W.A.; Verhoest, N.E.C. GLEAM v3: Satellite-based land evaporation and root-zone soil moisture. *Geosci. Model Dev.* **2017**, *10*, 1903–1925. [CrossRef]
51. Rodell, M.; Houser, P.R.; Jambor, U.; Gottschalck, J.; Mitchell, K.; Meng, C.J.; Arsenault, K.; Cosgrove, B.; Radakovich, J.; Bosilovich, M.; et al. The Global Land Data Assimilation System. *Bull. Am. Meteorol. Soc.* **2004**, *85*, 381–394. [CrossRef]
52. Dee, D.P.; Uppala, S.M.; Simmons, A.J.; Berrisford, P.; Poli, P.; Kobayashi, S.; Andrae, U.; Balmaseda, M.A.; Balsamo, G.; Bauer, P.; et al. The ERA-Interim reanalysis: Configuration and performance of the data assimilation system. *Q. J. R. Meteorol. Soc.* **2011**, *137*, 553–597. [CrossRef]

53. Han, C.; Ma, Y.; Wang, B.; Zhong, L.; Ma, W.; Chen, X.; Su, Z. Long-term variations in actual evapotranspiration over the Tibetan Plateau. *Earth Syst. Sci. Data* **2021**, *13*, 3513–3524. [CrossRef]
54. Muñoz-Sabater, J.; Dutra, E.; Agustí-Panareda, A.; Albergel, C.; Arduini, G.; Balsamo, G.; Boussetta, S.; Choulga, M.; Harrigan, S.; Hersbach, H.; et al. ERA5-Land: A state-of-the-art global reanalysis dataset for land applications. *Earth Syst. Sci. Data* **2021**, *13*, 4349–4383. [CrossRef]
55. Hersbach, H.; Bell, B.; Berrisford, P.; Hirahara, S.; Horanyi, A.; Munoz-Sabater, J.; Nicolas, J.; Peubey, C.; Radu, R.; Schepers, D.; et al. The ERA5 global reanalysis. *Q. J. R. Meteorol. Soc.* **2020**, *146*, 1999–2049. [CrossRef]
56. Dorigo, W.A.; Gruber, A.; De Jeu, R.A.M.; Wagner, W.; Stacke, T.; Loew, A.; Albergel, C.; Brocca, L.; Chung, D.; Parinussa, R.M.; et al. Evaluation of the ESA CCI soil moisture product using ground-based observations. *Remote Sens. Environ.* **2015**, *162*, 380–395. [CrossRef]
57. Entekhabi, D.; Njoku, E.G.; O'Neill, P.E.; Kellogg, K.H.; Crow, W.T.; Edelstein, W.N.; Entin, J.K.; Goodman, S.D.; Jackson, T.J.; Johnson, J.; et al. The Soil Moisture Active Passive (SMAP) Mission. *Proc. IEEE* **2010**, *98*, 704–716. [CrossRef]
58. Colliander, A.; Jackson, T.J.; Bindlish, R.; Chan, S.; Das, N.; Kim, S.B.; Cosh, M.H.; Dunbar, R.S.; Dang, L.; Pashaian, L.; et al. Validation of SMAP surface soil moisture products with core validation sites. *Remote Sens. Environ.* **2017**, *191*, 215–231. [CrossRef]
59. Reichle, R.H.; De Lannoy, G.J.M.; Liu, Q.; Ardizzone, J.V.; Colliander, A.; Conaty, A.; Crow, W.; Jackson, T.J.; Jones, L.A.; Kimball, J.S.; et al. Assessment of the SMAP Level-4 Surface and Root-Zone Soil Moisture Product Using In Situ Measurements. *J. Hydrometeorol.* **2017**, *18*, 2621–2645. [CrossRef]
60. Wei, M.Y. A new formulation of the exchange of mass and trace constituents between the stratosphere and troposphere. *J. Atmospheric Sci.* **1987**, *44*, 3079–3086. [CrossRef]
61. Immerzeel, W.W.; van Beek, L.P.H.; Bierkens, M.F.P. Climate Change Will Affect the Asian Water Towers. *Science* **2010**, *328*, 1382–1385. [CrossRef]
62. Piao, S.; Ciais, P.; Huang, Y.; Shen, Z.; Peng, S.; Li, J.; Zhou, L.; Liu, H.; Ma, Y.; Ding, Y.; et al. The impacts of climate change on water resources and agriculture in China. *Nature* **2010**, *467*, 43–51. [CrossRef]
63. Yu, L.; Fatichi, S.; Zeng, Y.; Su, Z. The role of vadose zone physics in the ecohydrological response of a Tibetan meadow to freeze-thaw cycles. *Cryosphere* **2020**, *14*, 4653–4673. [CrossRef]
64. Wigneron, J.P.; Jackson, T.J.; O'Neill, P.; De Lannoy, G.; de Rosnay, P.; Walker, J.P.; Ferrazzoli, P.; Mironov, V.; Bircher, S.; Grant, J.P.; et al. Modelling the passive microwave signature from land surfaces: A review of recent results and application to the L-band SMOS & SMAP soil moisture retrieval algorithms. *Remote Sens. Environ.* **2017**, *192*, 238–262. [CrossRef]
65. Kerr, Y.H.; Waldteufel, P.; Richaume, P.; Wigneron, J.P.; Ferrazzoli, P.; Mahmoodi, A.; Al Bitar, A.; Cabot, F.; Gruhier, C.; Juglea, S.E.; et al. The SMOS Soil Moisture Retrieval Algorithm. *IEEE Trans. Geosci. Remote Sens.* **2012**, *50*, 1384–1403. [CrossRef]
66. de Rosnay, P.; Munoz-Sabater, J.; Albergel, C.; Isaksen, L.; English, S.; Drusch, M.; Wigneron, J.-P. SMOS brightness temperature forward modelling and long term monitoring at ECMWF. *Remote Sens. Environ.* **2020**, *237*. [CrossRef]
67. Stewart, R.E.; Szeto, K.K.; Bonsal, B.R.; Hanesiak, J.M.; Kochtubajda, B.; Li, Y.; Theriault, J.M.; DeBeer, C.M.; Tam, B.Y.; Li, Z.; et al. Summary and synthesis of Changing Cold Regions Network (CCRN) research in the interior of western Canada - Part 1: Projected climate and meteorology. *Hydrol. Earth Syst. Sci.* **2019**, *23*, 3437–3455. [CrossRef]
68. DeBeer, C.M.; Wheater, H.S.; Pomeroy, J.W.; Barr, A.G.; Baltzer, J.L.; Johnstone, J.F.; Turetsky, M.R.; Stewart, R.E.; Hayashi, M.; van der Kamp, G.; et al. Summary and synthesis of Changing Cold Regions Network (CCRN) research in the interior of western Canada - Part 2: Future change in cryosphere, vegetation, and hydrology. *Hydrol. Earth Syst. Sci.* **2021**, *25*, 1849–1882. [CrossRef]